



# Methodology for mapping soil salinity and halophyte cover using remote sensing data in Kerkennah, Tunisia

Anna Igorevna Kurbatova<sup>1</sup> · Rim Attya Bouchhima<sup>2</sup> · Elizaveta Andreevna Grigorets<sup>1</sup> · Petr Romanovich Tsymbarovich<sup>3</sup> · Mohamed Ksibi<sup>2</sup>

Received: 23 June 2020 / Accepted: 16 March 2021

© Springer Nature Switzerland AG 2021

## Abstract

A global increase in average annual temperatures above land and oceans has led to increasing sea levels, which has in turn caused flooding along the coastlines of the Kerkennah Islands, Sfax Governorate, Central-East Tunisia. Seawater actively seeps into the groundwater of these islands. This groundwater is used for crop irrigation, which has resulted in rapid salinization and degradation of the soil cover. Thus, the environment in the Kerkennah Islands is characterized by hypersaline soil that is densely populated by halophytes. The halophyte distribution can be studied by mapping and monitoring using a remote sensing approach. In this work, we focused on determining the normalized difference vegetation index, the automated water extraction index, and the salinity index (NDVI, AWEI, and SI, respectively) in images obtained by Landsat 8 in order to map the soil salinity and halophyte cover in this region using the QGIS, GDAL, and SAGA GIS software packages. To achieve accurate land cover mapping of the Kerkennah Islands, we devised a scheme for identifying halophytes according to a decision tree based on a spectral classification approach that exploits several spectral indices. A regression model was used to detect significant relationships between spectral indices and soil characteristics such as pH and EC. The dynamics of the soil salinity in the study region were estimated using SI<sub>9</sub>, as this approach is known to give accurate results. The results confirm the methodology for mapping salinity by halophytes.

**Keywords** SI · NDVI · AWEI · Salinity · Halophyte cover · Mapping · Electroconductivity

## Introduction

Salinization is a universal problem that poses a serious threat to sustainable agricultural production. It has been estimated that almost 3 ha of arable land becomes unproductive every minute due to salinization aggravated by factors

such as water scarcity, drought, and the degradation of water resources (Lyra et al. 2014). Since the 1950s, significant changes to precipitation patterns have been observed in the Mediterranean area, along with rising sea levels and increasing temperatures and evapotranspiration (Brochier and Ramieri 2001).

Southern Tunisia is characterized by a desert arid climate and a large number of coastal sabkha (salt flat) areas. The piezometric levels of the deep water table of Sfax, which extends under the Kerkennah archipelago, seem to be decreasing, which may be due to the salinization of this aquifer caused by marine intrusion (Trabelsi et al. 2005). This causes the general flora of the island to consist mainly of tall xerophytes and often halophytes, such as palms and saltbushes. Sabkhas are also affected by salinity; these ecosystems are generally hypersaline environments that are crowded with halophytes.

Halophytes protect the shoreline from erosion and provide feeding areas for birds, fish, and animals. They are also camel provender (Mtmet 1999). These osmoprotective and

---

Responsible Editor: Anthony Lehmann.

Elizaveta Andreevna Grigorets  
5977749@mail.ru

<sup>1</sup> Faculty of Ecology, Peoples' Friendship University of Russia (RUDN University), 6, Miklukho-Maklaya Street, Moscow 117198, Russian Federation

<sup>2</sup> Laboratory of Environmental Engineering and Eco-Technology, National School of Engineers (ENIS), University of Sfax, Route de Soukra Km 3,5, P.O. Box 1173, 3038 Sfax, Tunisia

<sup>3</sup> Faculty of Soil Science, Lomonosov Moscow State University, 1, Leninskie Gory, Moscow 119991, Russian Federation

photoprotective properties of halophytes can be applied in cosmetology and health (Guillerme et al. 2017). Also, the ability to cultivate halophytes in a saline environment lacking fresh water (biosaline agriculture) can be valorized in the agrofood (human and animal food) industry. Halophytes can be used in phytoremediation, as they are capable of extracting heavy metals (Zn, Pb, Cu) from contaminated soils. The cleansed soils can then be used for conventional crops. They also play an interesting role in the greenification of salt marshes (Glenn et al. 1998; Hendricks and Bushnell 2008; Yensen 2008).

In addition, halophytes are considered major sources of a fuel that could replace fossil fuels (Debez et al. 2017). The raw materials used to produce alternative fuels for aviation are of biological origin and therefore renewable. Inedible oil crops such as halophytes are the main resources available for this fuel production process. Hendricks and Bushnell (2008) highlighted the great potential of halophytic plants for use as fuel-food feedstocks based on test plot data. According to a 2006 estimate by the US Energy Information Administration, 86% of the estimated 471.8 EJ of energy consumed globally in 2004 was provided by fossil fuels.

According to the literature, the types and the distribution of halophytes present on the Kerkennah Islands off the coast of Tunisia have barely been studied due to the vastness and inaccessibility of this territory. A remote sensing approach would appear to be very suitable for obtaining this information. Multispectral remote sensing would enable the identification of large-scale and hard-to-reach halophytic vegetation in southern Tunisia and its islands. Knowledge of the halophyte distribution would then allow areas affected by salt to be monitored and mapped (Bouaziz et al. 2011). Thus, in the work reported here, in order to obtain reliable and representative results for the distribution of halophytes and the salinity of the soils in the Kerkennah Islands, a multidisciplinary approach using remote sensing methods, spectral indices, a decision tree, and physicochemical analyses was implemented. In addition, surveys and field observations to identify halophytes in the study region were carried out.

Accurate projections of the halophytic vegetation in the archipelago can provide insight into the amount of salinity in the soils of this region, which is useful when attempting to map the spatial distribution of the salinity. Soil salinity has been estimated using vegetation reflectance in numerous studies, and many of them utilized vegetation indices, especially the normalized difference vegetation index (NDVI) (Tilley et al. 2007). It is important to mention that the most extensive research into soil salinization in the Kerkennah Islands was performed by Etienne (2014) using a GIS. That research showed that the islands are highly vulnerable to soil salinization and highlighted the growth of sabkhas due to changes in the climate and rising sea levels. The authorities subsequently established a new water policy that controlled

the use of brackish water for irrigation (Etienne 2014), so this study also attempted to assess the effect of this new policy on soil salinization in the study area. Researchers such as Huete and Liu (1994) and Leprieur et al. (2000) have claimed that the NDVI is very useful for mapping the distribution of halophytic vegetation. However, it is important to determine the applicability of various other spectral indices, such as the salinity index (SI), and to use these spectral indices in combination with vegetation indices to develop phenological detection techniques based on remote sensing. The results obtained using such an approach can then be compared with previous findings based on the NDVI.

Therefore, the main objectives of this study were to establish a methodological framework for mapping halophytes using soil indices in combination with vegetation indices and to assess the dynamics of the salinization of the Kerkennah Islands during the period 2013–2019. A protocol based on the analysis of a Landsat 8 image to study the distribution of halophytes on the islands was devised and validated. We compared various salinity indices that could be used to detect and map the halophyte cover in the area of interest in order to identify the salinity index that is best suited to determining the salinity on the ground using a decision tree algorithm.

## Material and methods

### Study area

The Kerkennah Islands are located in the Gulf of Gabes, 20 km off the Sfaxian coast ( $34^{\circ}42'N$ ,  $11^{\circ}10'E$ ). This archipelago consists of five small islands (between 0.5 and  $100\text{ km}^2$  in area), of which the two largest are Gharbi ( $48\text{ km}^2$ ) and Chergui ( $99\text{ km}^2$ ), and about ten very small islands (less than  $0.5\text{ km}^2$  in size) located northeast of Chergui (Fig. 1). The population of the Kerkennah Islands resides on Gharbi and Chergui. The islands are characterized by very low topographic relief, shallow soils that are susceptible to erosion, a semi-arid climate, and limited agricultural potential.

The maximum altitude of the islands is only 13 m above the sea, and the lowlands (less than 2.5 m above sea level) represent more than 50% of the islands (Etienne et al. 2012). The air temperature during the year ranges from +17 to +33 °C, and the water temperature from +15 to +28 °C. Seawater has noticeable mechanical and chemical effects on the soil of the islands due to its high tendency to erode: the soil is clay with gypsum inclusions, and is covered with a calcareous layer (Etienne 2014). A geological map of the Kerkennah Islands (Fig. 2) shows a preponderance of unconsolidated formations, in particular

**Fig. 1** The location of the Kerkennah archipelago

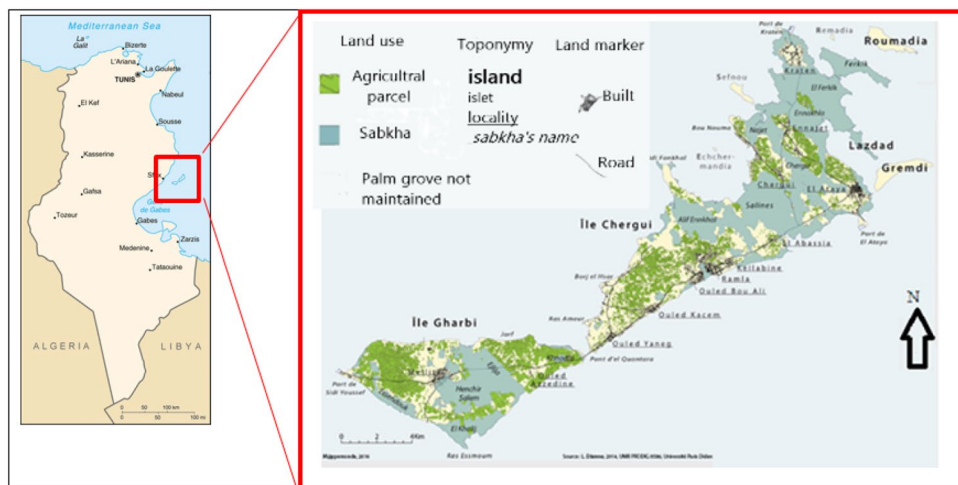
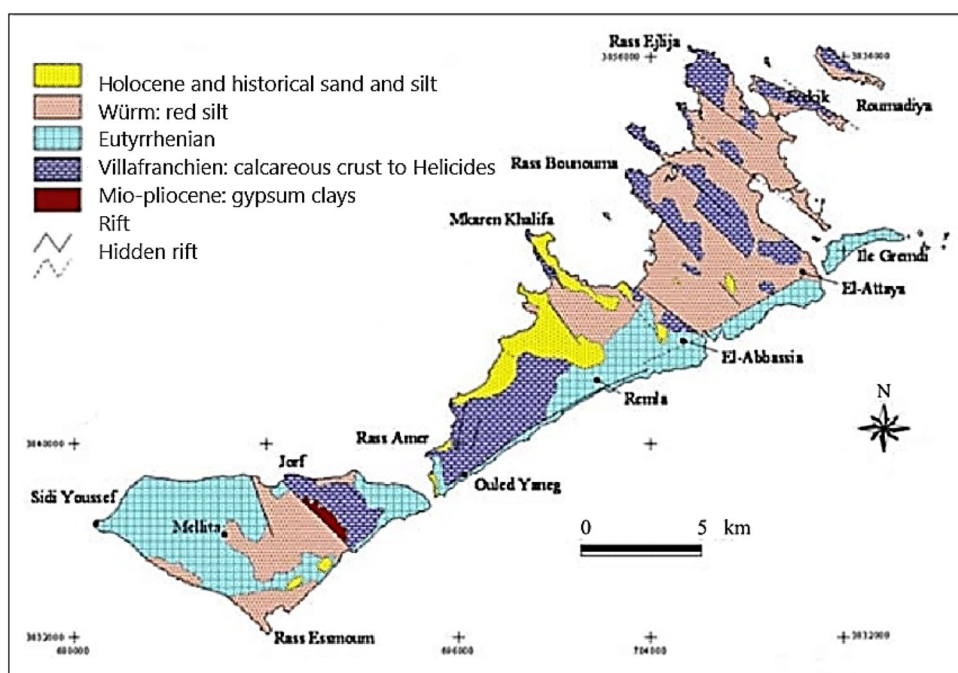


**Fig. 2** Geological map of the Kerkennah archipelago



the red silts of the Würm, which extend over about 39% of the total area of the archipelago (Fehri 2011).

The archipelago is unaffected by urbanization. The basis of its economy is fishing for export to the mainland, as well as small livestock and agriculture, represented by the cultivation of olive trees, dates, etc.

As Etienne (2017) noted, the soil salinity on the islands deserves special attention due to the agricultural activity in this territory, which is being hampered by rising sea levels, increasing average annual temperatures, outdated farming methods, and rainwater drainage. The lowlands of this archipelago are sporadically populated by halophytes. These lowlands are mostly connected to the sea

and include coastal sabkhas, which favor the growth of halophytic plants along their margins.

The use of satellite images and GIS would permit better monitoring of the archipelago's land cover, thus allowing the effectiveness of management policies for this attractive but vulnerable region to be improved. Indeed, Etienne (2014) demonstrated that the area covered by sebkhas on the islands is increasing, and that the salinity and death of vegetation along the margins is intensifying. Étienne et al. (2015) used two Landsat 4 and 5 TM images to compare the surface conditions on the islands in summer 1987 to those in summer 2009.

In 2011, the areas affected by salinization in southern Tunisia were mapped, thus allowing the halophyte distribution to be discerned (Bouaziz et al. 2011). Bouafif and Langar (2015) improved the mapping of some biocenoses in the Kerkennah Islands by processing an orthorectified (DIMAP format) image with a resolution of 0.5 m (pixel) obtained from the Pleiades satellite.

Fehri (2011) developed an approach that uses satellite imagery to study the causes of the spread of sebkhas across the Kerkennah Islands. He showed that this spread is due to physical processes that are triggered and/or aggravated by anthropogenic actions. This work allowed him to propose a better evaluation of the spatial dimension of this phenomenon.

In contrast to the investigations mentioned above, the study reported here considered not only the soil salinization and sabkha expansion in the study area but also the dynamics of the spread of halophyte cover. Unlike Etienne (2014), our research probed whether changes identified at the synoptic scale had visible repercussions for the archipelago. In addition, a field study was carried out in March 2010 to validate the typology.

## Data set

Landsat 8 data were used to investigate the land cover status. Landsat 8 Operational Land Imager (OLI) images were downloaded from the USGS (<http://glovis.usgs.gov> and <https://earthexplorer.usgs.gov>). The preprocessing method for Level 1 data in GeoTIFF format with Universal Transverse Mercator (UTM) projection and the WGS84 datum (Mtibaa and Irie 2016) was used. The study was performed during the summer period to get the highest salinity proportions and cloud-free images. Atmospheric corrections were processed using a digital elevation model (DEM) and ground reference information. The digital number of each pixel obtained from satellite imagery was converted to the Top of Atmosphere (TOA) value as shown below (ICCSA 2017):

$$\gamma_{\lambda} = \frac{M_p Q_{\text{cal}} + A_p}{\sin(\theta_{\text{SE}})}, \quad (1)$$

where  $\gamma_{\lambda}$  is the TOA reflectance for band  $\lambda$ ,  $M_p$  is the band-specific multiplicative rescaling factor,  $Q_{\text{cal}}$  is the quantized and calibrated standard product pixel value (DN),  $A_p$  is the band-specific additive rescaling factor, and  $\theta_{\text{SE}}$  is the local elevation angle of the sun in radians.  $M_p$ ,  $A_p$ , and  $\theta_{\text{SE}}$  are given in the metadata file provided in the Level 1 T data.

Five classes of land cover and vegetation were collected pixel by pixel using Google Earth: W, UBS, V, DV, and H, which represent water, urban and bare soil, vegetation, dense vegetation, and halophyte vegetation, respectively.

## Land cover mapping: spectral indices

NDVI mapping will effectively detect water bodies in most cases. However, it will often overestimate water bodies in the presence of urban, industrial, and infrastructural land cover, biasing the results obtained from NDVI mapping. This is why we used a different index, the automated water extraction index (AWEI), in this work.

Changes in the coastlines of the islands of the archipelago were examined for the period from 2013 to 2019 by mapping the AWEI (Feyisa et al. 2014). This index allows water objects to be more accurately distinguished from nonwater objects with low reflectivities (shadows or pixel noise) than when the NDVI is used. Various researchers (Feyisa et al. 2014; Colak et al. 2019; Kataev and Bekkerov 2017; Arreola Esquivel et al. 2019) have proven that the AWEI performs well in this context, providing greater accuracy than other water indices. Feyisa et al. (2014) defined two types of AWEI:

|                            |                                                                                                                               |
|----------------------------|-------------------------------------------------------------------------------------------------------------------------------|
| $\text{AWEI}_{\text{nsh}}$ | This is formulated to effectively eliminate non-water pixels, including dark built surfaces in areas with an urban background |
| $\text{AWEI}_{\text{sh}}$  | This is formulated to further improve discrimination accuracy by removing shadow pixels (especially in mountain regions).     |

In this work,  $\text{AWEI}_{\text{nsh}}$  was used, as the archipelago has a flat topography (lowering the chance of shading errors), and errors are most likely to be due to the presence of rare urban buildings. This index is calculated as follows (Feyisa et al. 2014):

$$\text{AWEI}_{\text{nsh}} = 4(\text{Green} - \text{SWIR1}) - (0.25 \text{ NIR} + 2.75 \text{ SWIR2}). \quad (2)$$

$\text{AWEI}_{\text{nsh}}$  maps were polygonized with the `gdal_polygonize.py` utility and provisioned manually to clean pixels with artifacts and to fix invalid geometries. These polygons were used to calculate the area covered by non-water objects.

The presence of salinity in the soil can be discerned from the presence of stressed vegetation such as halophytes. Soil salinity is usually affected by dispersed vegetation. Therefore, NDVI and SI were mapped to distinguish salt-affected soils.

Landsat data were processed as follows to give NDVI values that were subsequently employed to classify and compare the land cover types in each image (NASA Earth Observatory 2020):

$$\text{NDVI} = \frac{\text{NIR} - \text{R}}{\text{NIR} + \text{R}}. \quad (3)$$

The NDVI value for a given pixel is always in the range from  $-1$  to  $+1$ . Negative NDVI values are indicative of water, values of around zero represent bare soil, and values  $> 0.7$  represent dense green vegetation. To check the distinction between the calculated sites, the separability was verified by calculating the Jefries–Matusita distance for each pair of classes using the “Regions of interest (ROI) separability” function in ENVI (see Table 1).

A class with low separability from another class will be confused with it or should be redefined. In this work, the correlation between the vegetation index and local truth data was investigated using remote sensing images. Fernandez Buces et al. (2006) found that there was a significant correlation between NDVI, EC, and SAR in Mexico. In addition, Pérez González et al. (2006) correlated the NDVI of halophytic vegetation with the spatial variability of the chemical and physical properties of a site to identify saline hydro-morphic soils. Their results showed that the NDVI was very suitable for detecting halophytic plants and relating them to saline soils. In addition, Bannari et al. (2008) stated that since plant growth was slowed by soil salinity, salt stress could be predicted using the NDVI. However, researchers such as Metternicht and Zinck (2008) and Zhang et al. (2011) argue that it is difficult to detect soil salinity using NDVI because the presence of vegetation can cause spectral confusion with the reflectance properties of salt and because NDVI is considered an unreliable indicator given that it is correlated with other yield variables such as chlorophyll content, biomass, and leaf area.

The salinity of the soil is the amount of soluble salt retained in it. As the soil salinity increases, salt ions appear on the soil surface, which implies that remote sensing is useful for soil mapping. Over the past decade, multispectral data with a variety of spatial and temporal resolutions (e.g., data from Landsat, ASTER, MODIS, radar, etc.) have been used to monitor (Periasamy and Shanmugam 2017; Shrestha 2006; Wu et al. 2008) and map (Taghizadeh-Mehrjardi 2014; Yu et al. 2010) saline soils and halophytic vegetation (Bell et al. 2001; Sidike et al. 2014).

Derived from the green, red, and near-infrared bands, the salinity index (SI) was developed to map soil salinity to sparse vegetation cover (Douaoui et al. 2006). The SI

was calculated in order to assess the potential and limitations of remote sensing for the detection of soil salinity in the Kerkennah area. The electrical conductivity (EC) was used to measure the salinity of soil samples taken in the field. The correlation between the salinity measured in the field and soil spectral indices was calculated in order to assess differences in salinity in halophytic zones. According to Douaoui et al. (2006), the following three salinity indices are those that are most strongly correlated with soil salinity:

$$SI_1 = G/(R \times NIR) \quad (4)$$

$$SI_8 = \sqrt{G \times R} \quad (5)$$

$$SI_9 = \sqrt{G^2 + R^2 + NIR^2}. \quad (6)$$

These and all other raster calculations were performed with the gdal\_calc.py utility. All of the data used were filtered to be cloudless except for some clouds over the sea. To prevent these clouds from being classified as non-water, the Landsat 8 Quality Assessment Band (BQA) was used. Mask files of clear terrain were calculated with the formula below (USGS 2018):

$$\forall px : px_{BQA} \in \{2720, 2724, 2728, 2732\} \rightarrow px \in \text{ClearTerrain}. \quad (7)$$

In order to detect variables that are sensitive to the soil pH and EC, spectral analyses of soil samples were conducted. Several authors have already evaluated the relationships between the soil surface spectral response and soil physical and chemical properties for other territories (Bannari et al. 2008; Triki et al. 2017). Regression coefficients have been used to indicate the impacts of the independent variables on the dependent variable; the higher the value of the regression coefficient, the greater the impact on the dependent variable (Sidike et al. 2014). In this context, multiple linear regression (MLR) analysis was conducted in this study to investigate the influence of soil salinity on the EC, soil pH, and spectral indices. In this method, pH and EC were the independent variables and the values of the spectral indices (the dependent variables) were predicted. The performance of the model was evaluated by calculating  $R^2$ , which indicates the strength of the statistical correlation between the measured and predicted values. The model is considered to be (Farifteh et al. 2008):

- Accurate if  $R^2 > 0.91$
- Good if  $0.82 < R^2 < 0.90$
- Moderate if  $0.66 < R^2 < 0.81$
- Poor if  $0.5 < R^2 < 0.65$ .

**Table 1** Separability according to the value of  $X$

| $X$       | Separability                                                         |
|-----------|----------------------------------------------------------------------|
| $< 1.0$   | Very low separability; 0 implies total confusion between two classes |
| $< 1.9$   | Low separability                                                     |
| $1.9–2.0$ | Good separability                                                    |
| 2         | Perfect separability with no risk of confusion                       |

$X$  = the Jefries–Matusita distance

Thus, the linear regression model makes it possible to analyze the influences of the different variables used in the model in order to determine the best indices for predicting the level of soil salinity.

Calculating  $R^2$  allows the significance of the relationship to be determined by testing whether the pH and EC are conducive to the estimation of variables that are dependent on spectral indices (Hines and Montgomery 1990; Scherrer 1984). Relatively low values of the correlation coefficients of the empirical relationships indicate that using the pH or EC can lead to significant errors in the estimation of spectral indices.

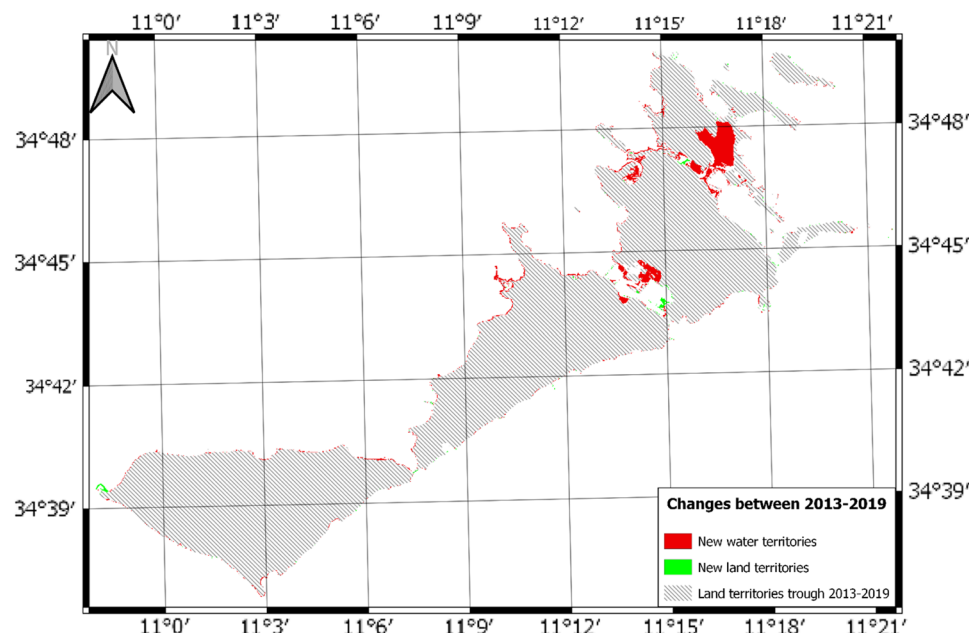
The overall precision and the kappa coefficient ( $k$ ) are useful indices of the accuracy of classification of remotely sensed data (Hudson and Ramm 1987; Congalton 1991; Alexandridis et al. 2008; Ndehedehe et al. 2013), and were used in this work to analyze the sensitivity of the methodology.

According to Cohen (1960), kappa values can be classified as shown in Table 2.

**Table 2** Classification of kappa values according to Cohen (1960)

| Range of $K$      | Classification         |
|-------------------|------------------------|
| $K \leq 0$        | No agreement           |
| $0.01 < K < 0.20$ | Overly weak agreement  |
| $0.21 < K < 0.40$ | Weak agreement         |
| $0.41 < K < 0.60$ | Moderate agreement     |
| $0.61 < K < 0.80$ | Strong agreement       |
| $0.81 < K < 1.00$ | Near-perfect agreement |

**Fig. 3** Map showing changes to water and nonwater surfaces in the Kerkennah archipelago during 2013–2019 (resolution: 30 m; coordinate system: WGS84)



## Results and discussion

### Water mapping

The nonwater surface area dynamics of the Kerkennah Islands were assessed using the AWEI<sub>nsh</sub>. As can be seen in Fig. 3, uniform flooding of coastal zones was observed throughout the islands, reducing the total land area. Statistical processing of the spectral index results yielded the values presented in Table 3.

The total loss of land area during the 2013–2019 was 3.4% (Fig. 4).

Moreover, the AWEI<sub>nsh</sub> calculations were used to create a nonwater area mask, which was then used to reduce possible errors when mapping the dynamics of SI<sub>9</sub> for the period 2013–2019. This step was necessary because the

**Table 3** Evolution of the nonwater surface area in the Kerkennah archipelago during 2013–2019

| Year | Area (km <sup>2</sup> ) | Area difference (km <sup>2</sup> ) | Area difference (%) |
|------|-------------------------|------------------------------------|---------------------|
| 2013 | 153.6                   | N/D                                | N/D                 |
| 2014 | 149.1                   | − 4.5                              | − 2.9               |
| 2015 | 152.0                   | 2.9                                | 1.9                 |
| 2016 | 152.1                   | 0.2                                | 0.1                 |
| 2017 | 149.7                   | − 2.4                              | − 1.6               |
| 2018 | 151.4                   | 1.7                                | 1.1                 |
| 2019 | 148.3                   | − 3.1                              | − 2.0               |

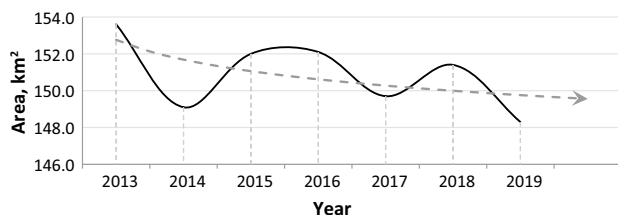


**Fig. 4** Graph showing the change in the total nonwater surface area in the Kerkennah Islands

**Fig. 5** Normalized difference vegetation index (NDVI) attributes across the ROI on 26/07/2015 (resolution: 30 m; coordinate system: WGS84)

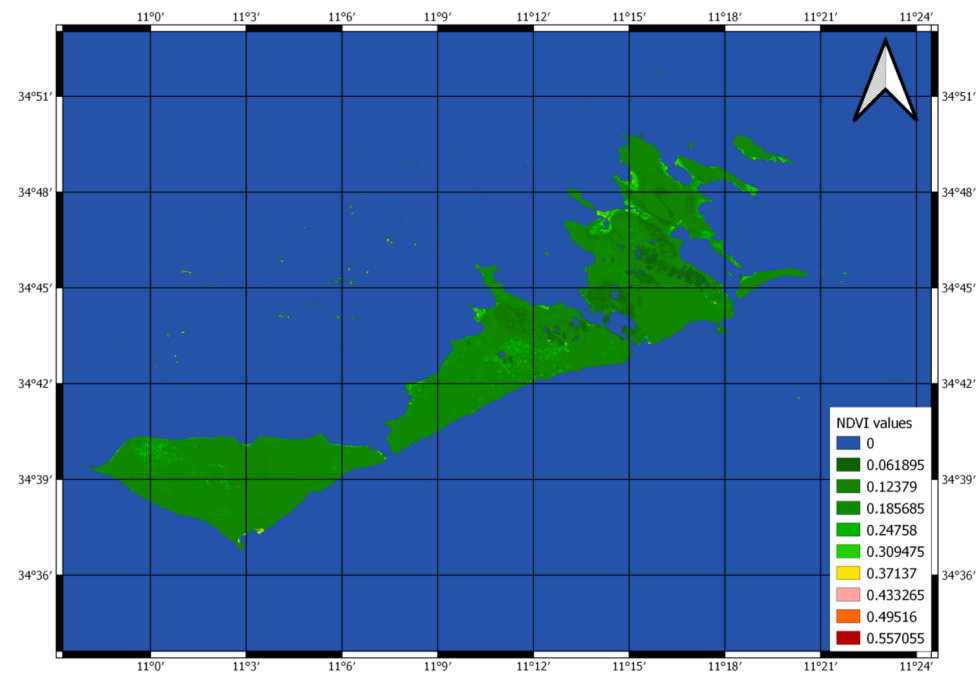
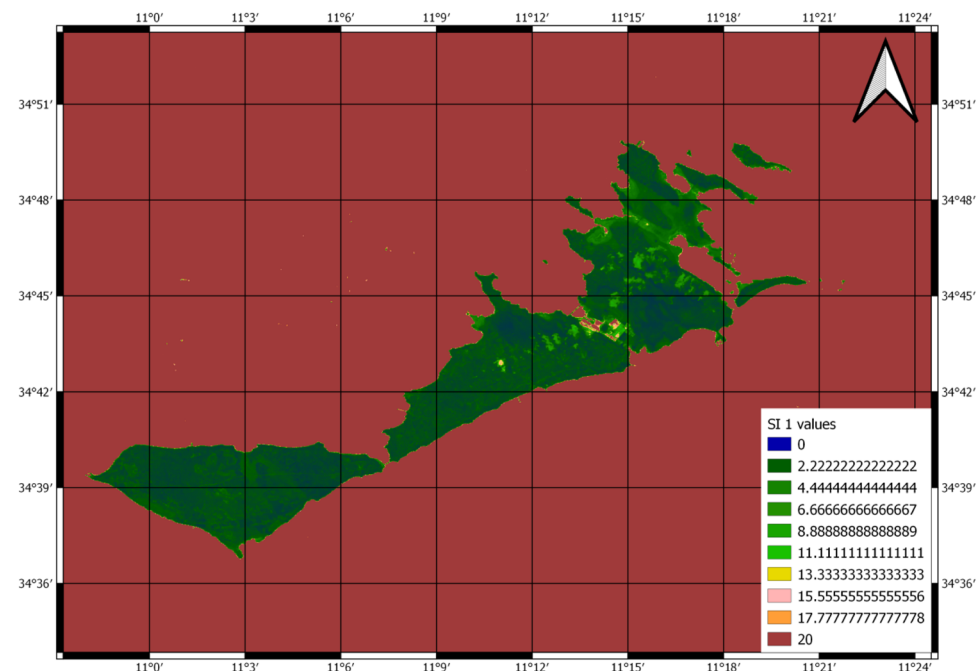


**Fig. 6** Attributes of the salinity index SI<sub>1</sub> across the ROI on 26/07/2015 (resolution: 30 m; coordinate system: WGS84)



region has a dry climate and water could be poorly classified by nonwater indices.

### Land cover mapping

The NDVI and SIs were calculated, and the resulting graphical maps are presented in Figs. 5, 6, 7, 8.

The normal NDVI value for water bodies is 0. NDVI values for vegetation cover are in the range 0.15–0.3, allowing

**Fig. 7** Attributes of the salinity index  $SI_8$  across the ROI on 26/07/2015 (resolution: 30 m; coordinate system: WGS84)

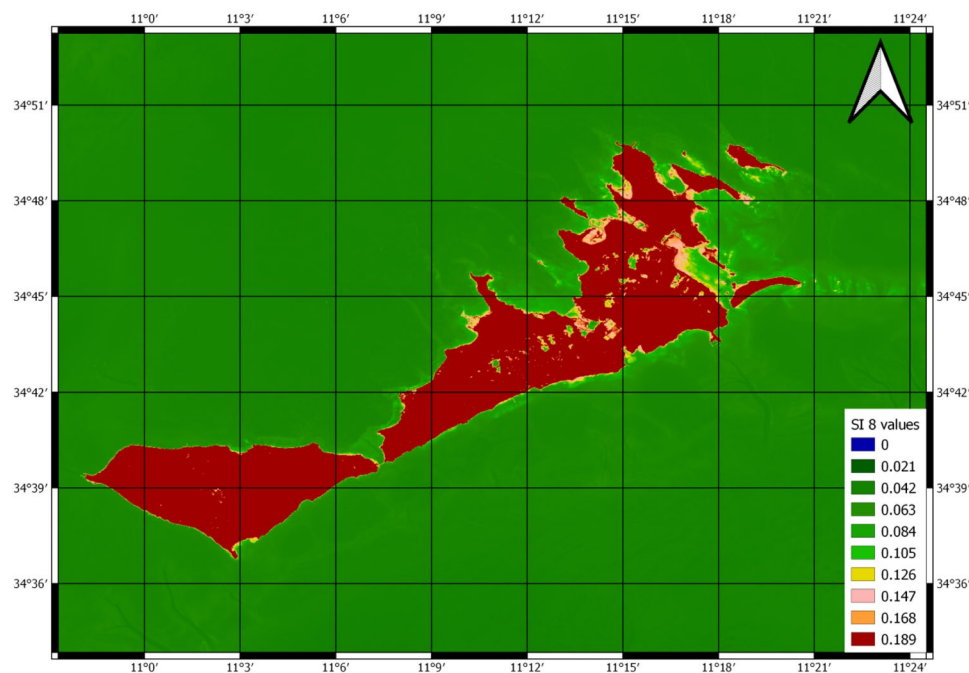
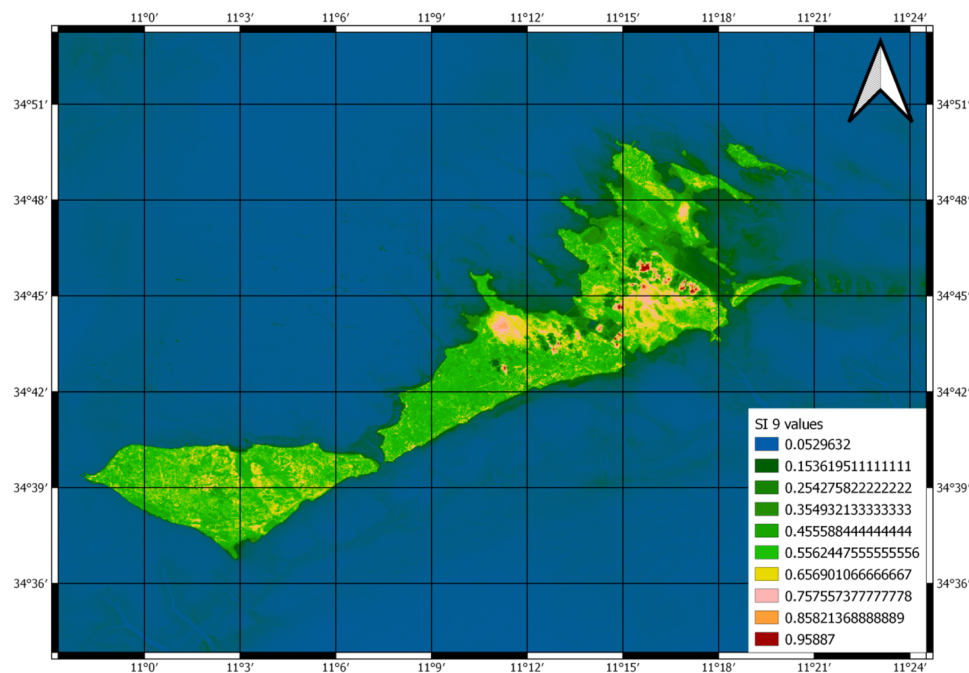


**Fig. 8** Attributes of the salinity index  $SI_9$  across the ROI on 26/07/2015 (resolution: 30 m; coordinate system: WGS84).



this cover class to be reliably discriminated from another cover class (Abu Qdais and Shatnawi 2019; Llerena et al. 2019; Shatnawi and Abu Qdais 2019). The results obtained when the areas were classified by spectral indices are grouped in Table 4.

After performing the separability calculation, we obtained the results listed in Table 5.

The values obtained indicated that the classification was successful.

**Table 4** Ranges of NDVI,  $SI_1$ ,  $SI_8$  and  $SI_9$  for the different cover classes, based on field visits and spectral signatures identified in the Landsat 8 image from 26 July 2015

| Index  | Halophytes | Sea  | Bare soil |
|--------|------------|------|-----------|
| NDVI   | 0.15–0.3   | 0    | 0.1–0.15  |
| $SI_1$ | 4–11       | 20   | 0–4       |
| $SI_8$ | 0.1        | 0.07 | 0.16      |
| $SI_9$ | 0.3–0.95   | 0    | 0.1–0.3   |

**Table 5** Spectral distances calculated according to the separability calculation method

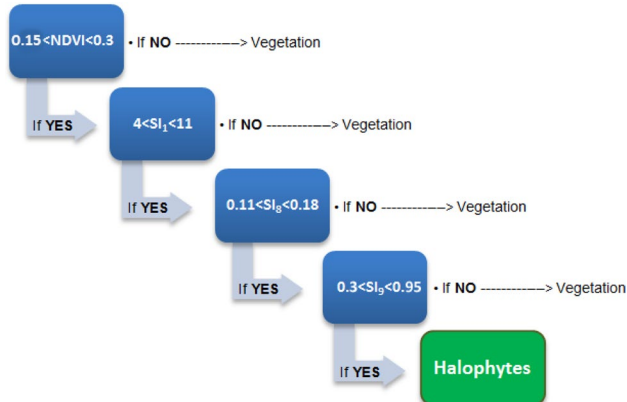
| X              | Description                    |
|----------------|--------------------------------|
| 0.70106829     | Halophytes and bare soil       |
| 0.77623228     | Bare soil and very saline soil |
| 1.999999999999 | Highly saline sea and soil     |
| 2.00000000     | Sea and bare soil              |
| 2.00000000     | Sea and halophytes             |

The aim was to select halophytic areas based on integral usage of several indices (NDVI and the various SIs). To achieve this, the decision tree shown in Fig. 9 was used. This tree was first tested in an earlier study by Attya et al. (2018) as a means to estimate the halophyte cover around Ghannouch, Tunisia.

Each condition consists of a qualifying statement. Each time a condition is met, the resulting binary map/class is excluded from the potential halophyte zone, resulting in a final map of areas suitable for halophyte coverage. A set of land cover classes of interest was defined: urban and bare soil, vegetation, dense vegetation, and halophytic vegetation. The criteria and thresholds are described in the order in which they are encountered in the decision tree. The final decision tree included four variables that were considered to be the most effective indicators of areas not suitable for halophytic coverage. The results obtained make it possible to distinguish halophyte zones, as was done previously by Attya et al. (2018) for the halophytic cover around Ghannouch, Tunisia.

### Classification of halophytic cover

Spatial variability and soil quality are the limiting factors when assessing and mapping halophytes using remotely sensed data. This is because spectral reflectance

**Fig. 9** Decision tree based on criteria and index thresholds

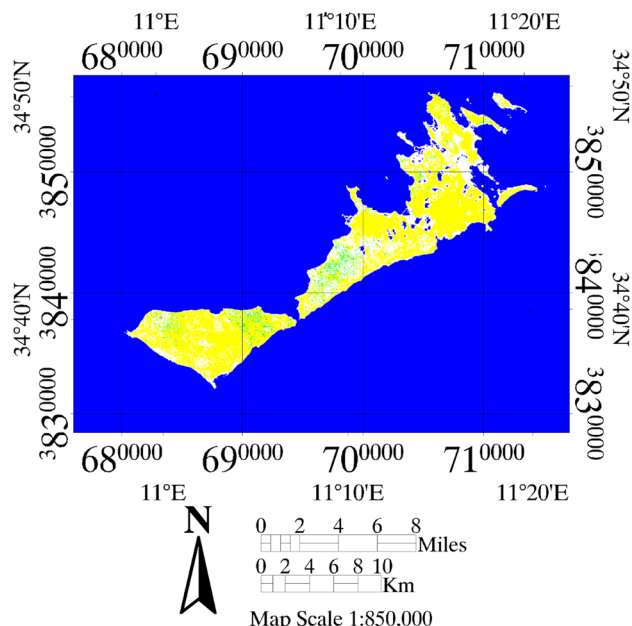
cannot provide information on the entire soil profile—it only observes the ground surface. Furthermore, in many cases, surface characteristics may not be representative of the conditions deeper in the soil (Dewitte et al. 2012). Thus, the combination of remote sensing with soil salinity studies is key to the accurate mapping of the halophyte population.

In addition, different types of vegetation typically grow at different salinity levels, so the NDVI is considered an unreliable indicator for monitoring and mapping soil salinity. To overcome this limitation of remote sensing, a proxy indicator was used to map halophytes: the soil salinity status was monitored using the NDVI and the SI. Utilizing a combination of the NDVI and the SI via the QGIS platform, a halophyte classification map for the Kerkennah Islands was obtained (Fig. 10).

These results confirm that the sea level is increasing, which could play a role in the soil salinization of the islands of the Kerkennah archipelago, as noted by Etienne (2017).

The islands are surrounded by seawater, represented by the blue for water, yellow for bare soil, green for halophytes in Fig. 10. Bare land is shown in green in this figure. High-salinity areas occur at the northeastern end of the archipelago (Kraten), and are dominated by the presence of sabkhas. Halophytic species, the presence of which is indicated by a red color, predominate in the center of the archipelago as well as downstream of the island of Chargui in the northeast.

These halophyte and saline zone distributions are in accord with the results of previous studies by Dahech (2007) and Etienne et al. (2012). Those authors reported that recent

**Fig. 10** Halophyte mapping in the Kerkennah archipelago (regions with halophytes are shown in green)

shifts in regional climatic and environmental conditions, including sea level rises, temperature rises, and changes in rainfall and the wind regime are the main causes of the growth of sabkhas—favorable sites for halophytic plant growth—in this region.

### Soil chemistry results and interpretation

Chemical analyses of the soil showed that there was a correlation between the halophyte plant zones and the presence of saline soil. Chemical properties of the soil samples taken from the archipelago (Fig. 11) are summarized in Table 6. Sample 4 presented high conductivity and a relatively high level of organic matter. This organic matter is degraded by strong bacterial activity in the medium, leading to mineralization and hence high salinity.

Similarly, sample 7 is characterized by a high cation exchange capacity (CEC) of  $> 50$  mEq/100 g, meaning

that the soil is organic. The total organic carbon (TOC) value is very low  $< 5\%$ , indicating that the organic matter has been degraded, resulting in high salinity. The CEC is the preferred parameter for characterizing soil surface properties. Soil CEC characterization is useful for inferring the amounts of phosphorus, potassium, and magnesium in soils of different textures. All of the soil samples were found to have a high CEC, implying that ions are readily bound to the clay–humic complex.

Samples 4 and 7 showed the highest CEC values. The corresponding locations may be sites that are highly polluted with salt water.

Analysis of Landsat 8 OLI imagery is an appropriate and economical means to extract information on the soil salinity and sodicity of large areas. In general, the benefits of remote sensing include rapid access, reduced analysis time, wider coverage, and the availability of a consistent time series for long-term monitoring (Setia et al. 2013; Fan et al. 2015; Navarro-Pedreño et al. 2007).

**Fig. 11** Map of soil sampling locations (coordinate system: WGS84)

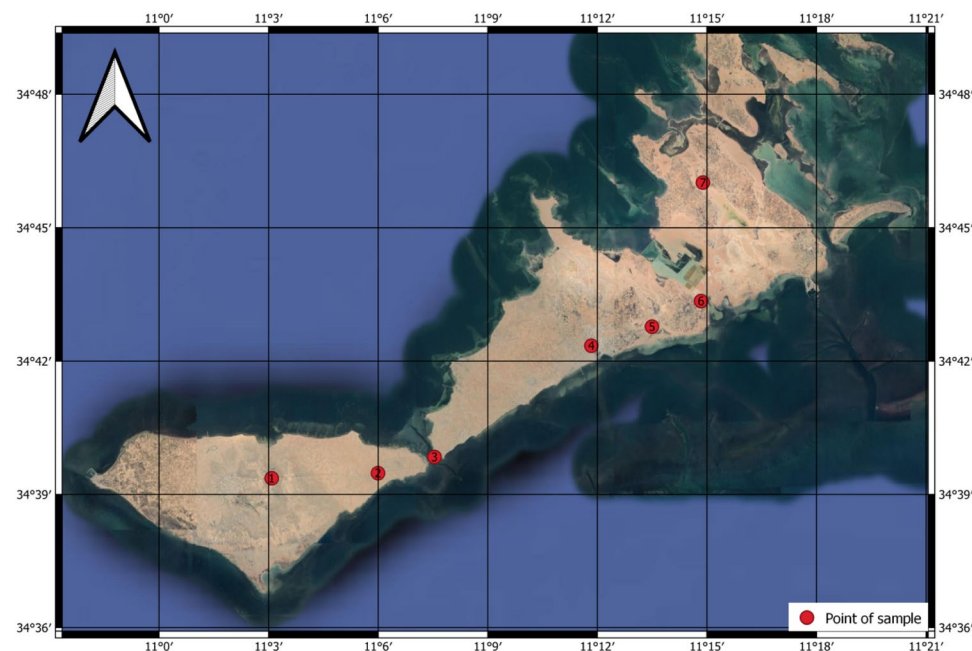


**Table 6** Chemical properties of soil samples from the Kerkennah Islands

| Samples | Latitude     | Longitude    | pH    | Conductivity (mS/cm) | T (°C) | CEC (mEq/100 g) | TOC (%) |
|---------|--------------|--------------|-------|----------------------|--------|-----------------|---------|
| 1       | 34°39'21.81" | 11°03'04.94" | 8.555 | 1.8415               | 15.5   | 11.76           | 0.32    |
| 2       | 34°39'28.7"  | 11°05'59.6"  | 8.98  | 6.705                | 15.7   | 37.10           | 1.47    |
| 3       | 34°39'50.5"  | 11°07'32.4"  | 9.23  | 1.6995               | 16     | 6.79            | 1.60    |
| 4       | 34°42'20.7"  | 11°11'50.0"  | 8.6   | 9.245                | 15.7   | 38.46           | 2.83    |
| 5       | 34°42'46.5"  | 11°13'29.6"  | 8.29  | 1.1665               | 15.7   | 29.18           | 0.44    |
| 6       | 34°43'21.1"  | 11°14'50.2"  | 8.77  | 2.11                 | 16.3   | 33.71           | 0.92    |
| 7       | 34°46'07.5"  | 11°13'15.5"  | 8.54  | 14.645               | 16.2   | 50.90           | 1.09    |

## Sensitivity analysis of the methodology

Based on the method reported by Douaoui et al. (2006) for correlation coefficient determination and the field measurements of EC and pH, the correlations of the spectral indices (NDVI, SI<sub>1</sub>, SI<sub>8</sub>, and SI<sub>9</sub>) with the pH and EC were evaluated in order to gauge the sensitivity of the methodology. Based on the correlation coefficients for the regression equations shown in Table 7, it is clear that the best correlation with EC and pH is achieved when SI<sub>9</sub> is used as the index ( $R^2=0.9$ ). The NDVI, SI<sub>1</sub>, and SI<sub>8</sub> yield  $R^2$  values of 0.4, 0.5, and 0.2, respectively. Thus, the index SI<sub>9</sub> is the best choice for assessing soil salinity and sodicity.

Laboratory analysis showed that the pH values of the soil samples ranged from 8.2 to 9.2, with a mean content of 8.70, which generally indicates sodium levels (Ali 2011). EC measurements of the samples ranged from 1.1 to 14.6 mS/cm, with an average of 5.3 mS/cm, indicating very high soluble salt concentrations. Thus, most of the soils in the study area were affected by high sodium and salinity levels. Table 7 shows the correlation coefficients between soil EC, pH, and all spectral indices. Table 8 shows that there are no significant correlations between these salinity indices and the halophytic vegetation represented by NDVI. This is likely due to the low density of vegetation cover in the study area. Indeed, it has been shown that the use of vegetation

indices for salinity assessment and mapping in areas with densely vegetated soils will give promising results, whereas this approach is not reliable for sparse or bare soils. The use of soil salinity indices is more appropriate for bare soils or soils with very low vegetation cover. These observations are in agreement with those of Bouaziz et al. (2011) and Fan et al. (2012).

Bouaziz et al. (2011) found that vegetation indices such as the SAVI, NDVI, and EVI were poorly correlated with EC due to insufficient vegetation cover density, whereas soil salinity indices showed stronger correlations with EC. In addition, Fan et al. (2012) found that the NDVI had a significant negative relationship with soil salinity in vegetated soils, whereas this relationship was unclear for bare soil.

Table 8 shows that SI<sub>1</sub> is positively correlated with pH, whereas SI<sub>9</sub> is negatively correlated with EC. SI<sub>1</sub> and SI<sub>8</sub> are negatively correlated with each other. Table 8 confirms the regression results for the spectral indices, EC, and pH. Note that this table shows that SI<sub>9</sub>, which gave the best value of  $R^2$  (0.9) among all of the spectral indices, is a good indicator for estimating the soil salinity and sodicity.

The results for soil EC and pH were classified into four levels of soil salinity (EC) and four levels of soil sodium (pH). In this research, EC values were found to be lower than those observed in some previous studies (Ali 2011; Taylor 1993; Zhang et al. 2011). Thus, soil salinity levels were classified according to Taylor (1993) and Zhang et al. (2011) as follows:

- EC < 0.2 mS/cm: not affected by salt
- 0.2 mS/cm < EC < 0.4 mS/cm: slightly saline
- 0.4 mS/cm < EC < 0.8 mS/cm: moderately saline
- EC > 0.8 mS/cm: intensely saline.

Soil sodium levels were classified according to Ali (2011) and Farifteh et al. (2008) as follows:

- pH < 8.5: nonsodic
- 8.5 < pH < 9.0: slightly sodic
- 9.0 < pH < 9.5: moderately sodic
- pH > 9.5: intensely sodic.

**Table 7** Regression equations for the spectral indices, pH, and EC

| Regression equation                 | Correlation coefficient ( $R^2$ ) |
|-------------------------------------|-----------------------------------|
| NDVI = 0.139 – 0.021 EC             | 0.4                               |
| NDVI = 0.139 – 0.018 pH             |                                   |
| SI <sub>1</sub> = –2.324 – 0.003 EC | 0.5                               |
| SI <sub>1</sub> = –2.324 + 2875 pH  |                                   |
| SI <sub>8</sub> = 0.561 – 0.003 EC  | 0.2                               |
| SI <sub>8</sub> = 0.561 – 0.461 pH  |                                   |
| SI <sub>9</sub> = 1.315 – 0.097 EC  | 0.9                               |
| SI <sub>9</sub> = 1.315 – 0.857 pH  |                                   |

**Table 8** Pearson correlation coefficients between spectral indices, soil pH, and EC (Carter 1993; Psilovikos and Elhag 2013; Tilley et al. 2007)

|                 | pH     | EC       | NDVI   | SI <sub>1</sub> | SI <sub>8</sub> | SI <sub>9</sub> |
|-----------------|--------|----------|--------|-----------------|-----------------|-----------------|
| pH              | 1      |          |        |                 |                 |                 |
| EC              | –0.206 | 1        |        |                 |                 |                 |
| NDVI            | 0.115  | –0.643   | 1      |                 |                 |                 |
| SI <sub>1</sub> | 0.702* | –0.167   | 0.332  | 1               |                 |                 |
| SI <sub>8</sub> | –0.459 | 0.000    | –0.392 | –0.773*         | 1               |                 |
| SI <sub>9</sub> | –0.074 | –0.896** | 0.646  | –0.072          | 0.300           | 1               |

\*\*Correlation is significant at the 0.01 level (bilateral)

\*Correlation is significant at the 0.05 level (bilateral)

The study area is mainly intensely saline and slightly sodic (Table 9). However, spectral reflectance was found to be nonsignificantly affected by variations in soil EC and pH. This implies that linear analysis of soil EC, pH, and spectral data is not feasible (Fig. 12).

**Table 9** Classifying the EC and pH values of the soil samples (Fan et al. 2015; Navarro-Pedreño et al. 2007; Setia et al. 2013)

| Sample | pH    | Sodium class     | EC     | Salinity class   |
|--------|-------|------------------|--------|------------------|
| 1      | 8.555 | Slightly sodic   | 1.8415 | Intensely saline |
| 2      | 8.98  | Slightly sodic   | 6.705  |                  |
| 3      | 9.23  | Moderately sodic | 1.6995 |                  |
| 4      | 8.6   | Slightly sodic   | 9.245  |                  |
| 5      | 8.29  | Nonsodic         | 1.1665 |                  |
| 6      | 8.77  | Slightly sodic   | 2.11   |                  |
| 7      | 8.54  | Slightly sodic   | 14.645 |                  |

Kappa coefficient and the overall precision are estimated based on the confusion matrix which was generated based on ROIs that were delineated using field data, photointerpretation, and spectral profiles.

Finally, our mapping results indicated that almost the entire region was affected by salt and sodium. However, the saline area was larger than the sodic area and the degree of soil salinity was greater than the degree of soil sodicity, as a small area of the islands presented moderately sodic soil whereas the entire saline area was intensely saline.

## Additional research

In addition, the dynamics of the soil salinity over the period 2013–2019 were assessed (see Table 10) based on  $SI_9$ , as this spectral index was found to give the strongest correlation with soil salinity.

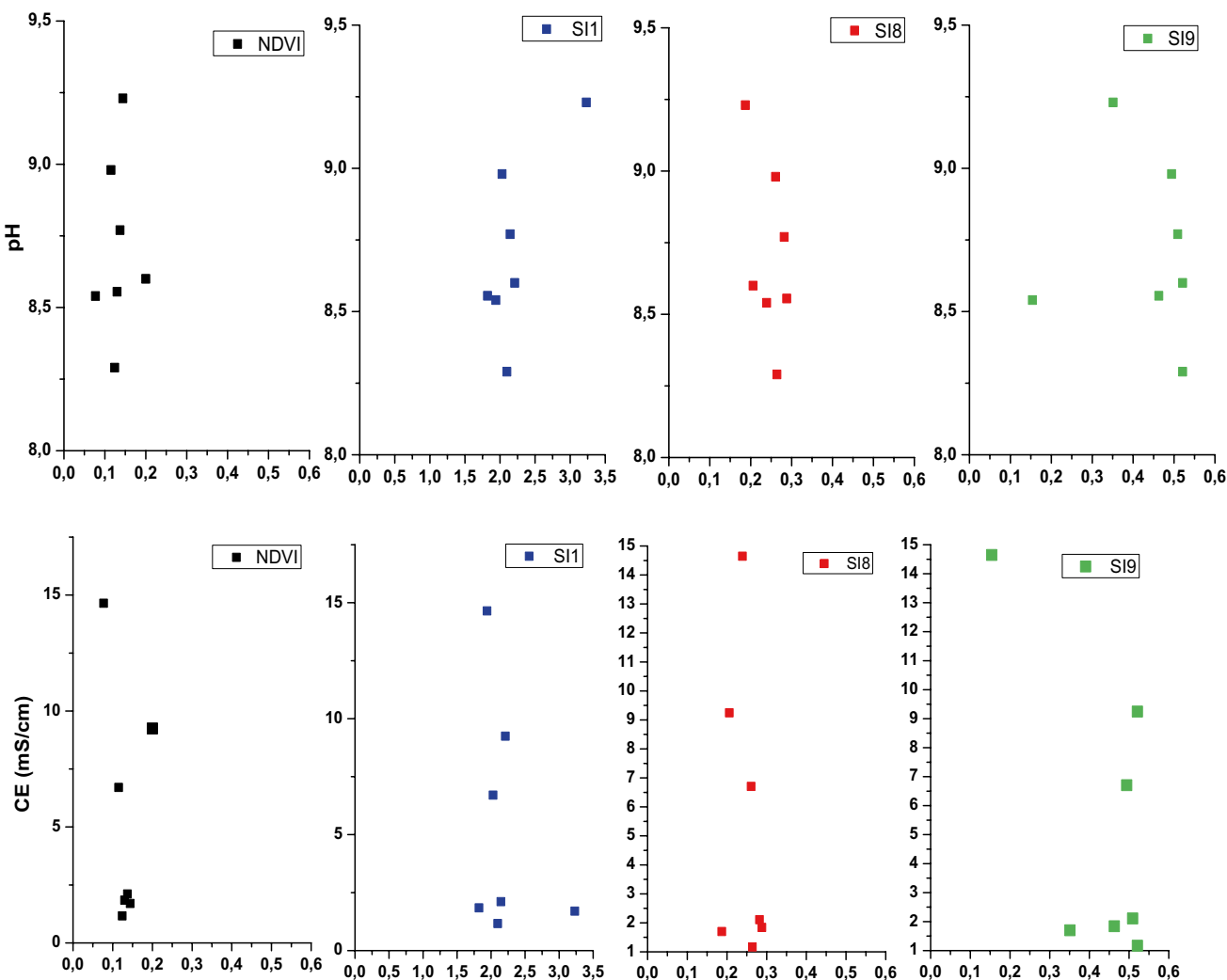


**Fig. 12** Correlations between the spectral indices (NDVI,  $SI_1$ ,  $SI_8$ , and  $SI_9$ ) and the measured soil EC or pH

**Table 10** Dynamics of the minimum, maximum, and mean  $SI_9$  values for the Kerkennah archipelago during the period 2013–2019

| Year | Min. $SI_9$ | Max. $SI_9$ | Mean $SI_9$ | St. deviation | Median |
|------|-------------|-------------|-------------|---------------|--------|
| 2013 | 0.128       | 0.87        | 0.55        | 0.08          | 0.56   |
| 2014 | 0.119       | 0.85        | 0.53        | 0.09          | 0.54   |
| 2015 | 0.127       | 0.78        | 0.48        | 0.08          | 0.49   |
| 2016 | 0.109       | 0.92        | 0.56        | 0.09          | 0.57   |
| 2017 | 0.124       | 0.92        | 0.50        | 0.08          | 0.51   |
| 2018 | 0.144       | 0.72        | 0.48        | 0.07          | 0.48   |
| 2019 | 0.135       | 0.88        | 0.49        | 0.08          | 0.50   |

**Table 11** Variation in the total area of saline soil (i.e.,  $SI_9 > 0.5$ ) in the Kerkennah Islands during the period 2013–2019

| Year | Estimated area of saline soil ( $\text{km}^2$ ) |
|------|-------------------------------------------------|
| 2013 | 112                                             |
| 2014 | 110                                             |
| 2015 | 64                                              |
| 2016 | 120                                             |
| 2017 | 83                                              |
| 2018 | 54                                              |
| 2019 | 78                                              |

The variation in the total area of saline soil during the period 2013–2019 is presented in Table 11.

Table 11 shows that the total area of saline soil in the archipelago is not stable and must be studied in combination with meteorological information and additional field trials. However, in general, the total area of saline soil in the archipelago appears to be decreasing. This decrease is likely to be due to the implementation of the new water policy that promotes the rational use of brackish water for irrigation, as mentioned by Etienne (2014).

## Limitations

Using remote sensing data can lead to errors due to the influence of the atmosphere and limits on instrument sensitivity, so the application of this methodology in other regions could result in lower accuracy.

Also, linking variables derived from Landsat 8 OLI to field measurements of salinity and sodicity did not make sense in this halophyte mapping methodology, the correlations do not have regular dynamics. Spectral reflectance was not found to be significantly influenced by variations in soil EC or pH. This implies that linear analysis of soil EC, pH, and spectral data is not feasible.

## Conclusion

The Kerkennah Islands in Tunisia are known to be vulnerable to climate change, given their very low elevations (maximum: 13 m) and high vulnerability to erosion. The sabkhas on these islands are known to be spreading, which may be due to climatic and environmental changes such as rising sea levels and subsidence. The presence of these sabkhas increases the risk of soil salinization on the islands. In further studies, the precise dependence of the sabkha distribution on meteorological and climatic parameters will be explored by analyzing the influence of temperature and humidity.

A regression model was used to determine the relationships between spectral indices and soil characteristics such as pH and EC for the Kerkennah Islands. Results showed that  $SI_9$  is the most accurate indicator of soil salinity and that spectral reflectance is not influenced by variations in soil EC and pH. A decision tree was developed to the aim was to select halophytic areas based on integral usage of several indices (NDVI and SI) and to distinguish halophytic zones using the QGIS platform. The performance of the methodology proposed in this study was evaluated by calculating the kappa coefficient (0.7) and overall accuracy (83%).

The water line of the archipelago was determined by mapping the  $AWEI_{\text{nsh}}$  in order to create a nonwater area mask for the period 2013–2019, which was used to reduce the soil salinity classification error. The soil salinity dynamics for this period were assessed using  $SI_9$ , which has proven accurate in this context.

To conclude, this work represents an initial contribution to the mapping of halophytes on the Kerkennah Islands, and involved testing and approving a decision tree using validation and precision parameters. Although the soil salinity in this region fluctuates, it must be controlled, as climatic and environmental changes are not decreasing. Taking measures to prevent further salinization will reduce the risk of soil degradation.

The use of salt-tolerant crops will not eliminate salt, so halophytes that have the ability to accumulate and exclude salt are desirable in this region. Halophyte phytoremediation is attractive as it can be performed very easily and at a low cost and at the same time, halophytes can be exploited as important plant species with the potential to desalinate and restore saline soils.

**Acknowledgments** The research was supported financially by the Russian Foundation for Basic Research (project no. 17-01-00693a). This work was also supported by the Tunisian Ministry of Higher Education and Scientific Research. This publication was prepared with the support of RUDN University Program 5-100.

## Declarations

**Conflict of interest** On behalf of all the authors, the corresponding author states that there is no conflict of interest.

## References

- Abu Qdais HA, Shatnawi N (2019) Assessing and predicting landfill surface temperature using remote sensing and an artificial neural network. *Int J Remote Sens* 40:9556–9571. <https://doi.org/10.1080/01431161.2019.1633703>
- Alexandridis TK, Zalidis GC, Silleos NG (2008) Mapping irrigated area in mediterranean basins using low cost satellite Earthobservation. *Comput Electron Agr* 64(2):93–103
- Arreola Esquivel A, Toxqui-Quitl C, Delgadillo M, Martin M (2019) Index-based methods for water body extraction in satellite data. *Proc SPIE* 11137. <https://doi.org/10.1117/12.2529756>
- Ali MH (ed) (2011) Springer Science + Business Media. Vol 2. LLC, New York, NY, USA, pp 271–325
- Attya R, Sarti M, Ciolfi M, Lauteri M, Ksibi M (2018) Decision tree for mapping of halophyte cover around Ghannouch. *Tunisia Environ Monitoring Assess* 190:742. <https://doi.org/10.1007/s10661-018-7115-3>
- Bannari A, Guedona AM, El-Hartib A, Cherkaouic FZ, El-Ghmi A (2008) Characterization of slightly and moderately saline and sodic soils in irrigated agricultural land using simulated data of advanced land imaging (EO-1) sensor. *Commun Soil Sci Plan* 39. <https://doi.org/10.1080/00103620802432717>
- Bell D, Menges C, Ahmad W, Zyl JJV (2001) The application of dielectric retrieval algorithms for mapping soil salinity in tropical coastal environment using airborne polarimetric SAR. *Remote Sens Environ* 75:375
- Bouaiffi C, Langar H (2015) Ecological study for the creation of a marine protected area in the north-eastern part of the Kerkennah Islands in Tunisia. Ed CAR/ASP—PNUE/PAM Replication Activity, Tunis
- Bouaziz M, Matschullat J, Gloaguen R (2011) Improved remote sensing detection of soil salinity from a semiarid climate in Northeast Brazil. *CR Geosci* 343(11–12):795–803
- Brochier F, Ramieri E (2001) Climate change impacts on the Mediterranean coastal zones. *SSRN Electron J*. <https://doi.org/10.2139/ssrn.277549>
- Carter GA (1993) Responses of leaf spectral reflectance to plant stress. *Am J Bot* 80(3):239–243
- Cohen J (1960) A coefficient of agreement for nominal scales. *Educ Psychol Meas* 20:37–46. <https://doi.org/10.1177/001316446002000104>
- Colak T, Senel G, Goksel C (2019) Coastline zone extraction using Landsat-8 OLI imagery, case study: Bodrum Peninsula, Turkey. In: 5th Int Conf Geoinformation Sci (GeoAdvances 2018), Casablanca, Morocco, 10–11 Oct 2018. <https://doi.org/10.5194/isprs-archives-XLII-4-W12-101-2019>
- Congalton RG (1991) A review of assessing the accuracy of classifications of remotely sensed data. *Remote Sens Environ* 37:35–46. [http://dx.doi.org/10.1016/0034-4257\(91\)90048-B](http://dx.doi.org/10.1016/0034-4257(91)90048-B)
- Dahech S (2007) Le vent à Sfax (Tunisie), impacts sur le climat et la pollution atmosphérique. Thèse de doctorat, université Paris VII, France, p 309
- Debez A, Belghith I, Friesen J, Montzka C, Elleuche S (2017) Facing the challenge of sustainable bioenergy production: could halophytes be part of the solution? *J Biol Eng* 11:27. <https://doi.org/10.1186/s13036-017-0069-0>
- Dewitte O, Jones A, Elbelrhiti H, Horion S, Montanarella L (2012) Satellite remote sensing for soil mapping in Africa an overview. *Prog Phys Geogr* 36(4):514–538
- Douaoui A, Hervé N, Christian W (2006) Detecting salinity hazards within a semiarid context by means of combining soil and remote-sensing data. *Geoderma* 134(1–2):217–230
- Etienne L (2014) Accentuation récente de la vulnérabilité liée à la mobilité du trait décote et à la salinisation des sols dans l'archipel de Kerkennah (Tunisie). PhD thesis. Université Paris Diderot (Paris 7)/Sorbonne Paris Cité/Université de Sfax, Paris/Paris/Sfax
- Etienne L (2017) La salinisation des sols dans l'archipel de Kerkennah, Tunisie. *Mappe Monde* 119
- Etienne L, Dahech S, Beltrando G, Daoud A (2012) Dynamiques récentes des sebkhas de l'archipel des Kerkennah (Tunisie centro-méridionale): apport de la télédétection. *Revue Télédétection*, 11(1):273–281
- Etienne L, Dahech S, Beltrando G, Daoud A (2015) Salinisation des sols et extension des sebkhas sur l'archipel de Kerkennah depuis 1963. In: *Vulnérabilité des littoraux méditerranéens face aux changements environnementaux contemporains*, Sfax, Tunisia, 20–24 Oct 2015, pp 105–110
- Fan X, Pedroli B, Liu G, Liu Q, Liu H, Shu L (2012) Soil salinity development in the yellow river delta in relation to groundwater dynamics. *Land Degrad dev* 23(2):175–189
- Fan X, Liu Y, Tao J, Weng Y (2015) Soil salinity retrieval from advanced multi-spectral sensor with partial least square regression. *Remote Sens* 7:488–511. <https://doi.org/10.3390/rs70100488>
- Farifteh J, Van Der Meer F, Van Der Meijde M, Atzberger C (2008) Spectral characteristics of salt-affected soils: a laboratory experiment. *Geoderma* 145:196–206. <https://doi.org/10.1016/j.geodrma.2008.03.011>
- Fehri N (2011) La palmeraie des îles Kerkennah (Tunisie), un paysage d'oasis maritime en dégradation: déterminisme naturel ou responsabilité anthropique? *Physio-Géo* 5:167–189. <https://doi.org/10.4000/physio-geo.2011>
- Fernández-Bucés N, Siebe C, Cram S, Palacio JL (2006) Mapping soil salinity using a combined spectral response index for bare soil and vegetation: a case study in the former lake Texcoco, Mexico. *J Arid Environ* 65(4):644–667. <https://doi.org/10.1016/j.jaridenv.2005.08.005>
- Feyisa GL, Meilby H, Fensholt R, Proud S (2014) Automated water extraction index: a new technique for surface water mapping using Landsat imagery. *Remote Sens Environ* 140:23–35. <https://doi.org/10.1016/j.rse.2013.08.029>
- Gervasi O, Murgante B, Misra S, Borruso G, Torre CM, Rocha AMAC, Taniar D, Apduhan BO, Stankova E, Cuzzocrea A (2017) Computational science and its applications—ICCSA 2017, part IV. Springer International, Cham
- Glenn EP, Brown JJ, O’Leary JW (1998) Irrigating crops with seawater. *Sci Am* 279:6–81
- Guillerme JB, Couteau C, Coiffard L (2017) Applications for marine resources in cosmetics. *Cosmetics* 2017(4):35. <https://doi.org/10.3390/cosmetics4030035>
- Hendricks RC, Bushnell DM (2008) Halophytes energy feedstocks: back to our roots. *ISROMAC* 12:20241
- Hines WW, Montgomery DC (1990) Probability and statistics in engineering and management science, 3rd edn. Wiley, New York
- Hudson W, Ramm C (1987) Correct formula of the kappa coefficient of agreement. *Photogramm Eng Remote Sensing* 53:421–422
- Huete AR, Liu HQ (1994) An error and sensitivity analysis of the atmospheric and soil-correcting variants of the NDVI for the MODIS-EOS. *IEEE Trans Geosci Remote Sens* 32:897–905
- Kataev M, Bekirov A (2017) Methodology of the water objects detection from multi-spectrum satellite measurements. *Proc TUSUR* 20:105–108. <https://doi.org/10.21293/1818-0442-2017-204-105-108>

- Leprieur C, Kerr YH, Mastorchio C (2000) Monitoring vegetation cover across semi-arid regions: comparison of remote observations from various scales. *Int J Remote Sens* 21(2):281–300. <https://doi.org/10.1080/014311600210830>
- Llerena S, Tarko A, Kurbatova A, Kozhevnikova P (2019) Assessment of carbon dynamics in Ecuadorian forests through the mathematical spatial model of global carbon cycle and the normalized differential vegetation index (NDVI). EDP Sciences, Les Ulis
- Lyra D, Ismail S, Rehman K (2014) Biosalinity News 15:6–7
- Metternicht G, Zinck A (2008) Remote sensing of soil salinization: impact on land management. CRC, Boca Raton
- Mtibaa S, Irie M (2016) Land cover mapping in cropland dominated area using information on vegetation phenology and multi-seasonal Landsat 8 images. *Euro-Mediterr J Environ Integr* 1:6. <https://doi.org/10.1007/s41207-016-0006-5>
- Mtimet A (1999) Atlas des Sols tunisiens. Ministère de l'Agriculture et des Ressources Hydrauliques de la Tunisie, Tunis
- Navarro-Pedreño J, Jordan MM, Meléndez-Pastor I, Gómez I, Juan P, Mateu J (2007) Estimation of soil salinity in semi-arid land using geostatistical model. *Land Degrad Dev* 18:339–353
- NASA Earth Observatory (2020) Measuring vegetation (NDVI & EVI). [https://earthobservatory.nasa.gov/features/MeasuringVegetation/measuring\\_vegetation\\_2.php](https://earthobservatory.nasa.gov/features/MeasuringVegetation/measuring_vegetation_2.php). Last accessed 15 Feb 2020
- Ndehedehe C, Ekpa A, Simeon O, Nse O (2013) Understanding the neural network technique for classification of remote sensing datasets. *NY Sci J* 6:26–33
- Pérez González ME, Rodríguez PG, Gonzalez-Quiñones V, Ballesta I (2006) Spatial variability of soil quality in the surroundings of a saline lake environment. *Environ Geol* 51(1):143–149. <https://doi.org/10.1007/s00254-006-0317-y>
- Periasamy S, Shanmugam RS (2017) Multispectral and microwave remote sensing models to survey soil moisture and salinity. *Land Degrad Dev* 28:1412–1425
- Psilovikos A, Elhag M (2013) Forecasting of remotely sensed daily evapotranspiration data over Nile Delta region, Egypt. *Water Resour Manag* 27(12):4115–4130
- Scherrer DG (1984) The wilderness experience. *Recreat Sports* 8(2):19–21. <https://doi.org/10.1123/nirsa.8.2.19>
- Setia R, Lewis M, Marschner P, Raja Segaran R, Summers D, Chittleborough D (2013) Severity of salinity accurately detected and classified on a paddock scale with high resolution multispectral satellite imagery. *Land Degrad Dev* 24:375–384. <https://doi.org/10.1002/ldr.1134>
- Shatnawi N, Abu Qdais HA (2019) Mapping urban land surface temperature using remote sensing techniques and artificial neural network modelling. *Int J Remote Sens Appl* 40:3968–3983. <https://doi.org/10.1080/01431161.2018.1557792>
- Shrestha RP (2006) Relating soil electrical conductivity to remote sensing and other soil properties for assessing soil salinity in northeast Thailand. *Land Degrad Dev* 17:677–689
- Sidiike A, Zhao S, Wen Y (2014) Estimating soil salinity in Pingluo county of China using Quickbird data and soil reflectance spectra. *Int App Earth Obs Geoin* 26:156–175
- Taghizadeh-Mehrjardi R, Minasny B, Sarmadian F, Malone BP (2014) Digital mapping of soil salinity in Ardakan region, central Iran. *Geoderma* 213:15–28
- Taylor S (1993) Dryland salinity-introductory extension notes, 2nd edn. Department of Conservation and Land Management, Perth, Australia
- Tilley DR, Ahmed M, Son JH, Badrinarayanan H (2007) Hyperspectral reflectance response of freshwater macrophytes to salinity in a brackish subtropical marsh. *J Environ Qual* 36(3):780–789
- Trabelsi R, Zaïri M, Smida H, Ben Dhia H (2005) Salinisation des nappes côtières: cas de la nappe nord du Sahel de Sfax. *Tunisie C R Géosci* 337:477–483
- Triki FH, Bouaziz M, Benzina M, Bouaziz S (2017) Modeling of soil salinity within a semi-arid region using spectral analysis. *Arab J Geosci* 12:11175–11182
- USGS (2018) Landsat Collection 1 Information. Level-1 quality assessment band. [https://www.usgs.gov/land-resources/nli/landsat/lands-at-collection-1-level-1-quality-assessment-band?qt-science\\_support\\_page\\_related\\_con=0#qt-science\\_support\\_page\\_related\\_con](https://www.usgs.gov/land-resources/nli/landsat/lands-at-collection-1-level-1-quality-assessment-band?qt-science_support_page_related_con=0#qt-science_support_page_related_con). Last accessed 23 Jan 2020
- Wu J, Vincent B, Yang J, Bouarfa S, Vidal A (2008) Remote sensing monitoring of changes in soil salinity: a case study in Inner Mongolia. *China Sensors* 8:7035–7049
- Yensen NP (2008) Halophyte uses for the twenty first century (Chap. 23). In: Ajmal Khan M, Weber DJ (eds) *Ecophysiology of high salinity tolerant plants*. Springer, Dordrecht, pp 367–396
- Yu R, Liu T, Xu Y, Zhu C, Zhang Q, Qu Z, Liu X, Li C (2010) Analysis of salinization dynamics by remote sensing in Hetao Irrigation District of North China. *Agric Water Manag* 97:1952–1960
- Zhang TT, Zeng SL, Gao Y, Ouyang ZT, Li B, Fang CM, Zhao B (2011) Using hyperspectral vegetation indices as a proxy to monitor soil salinity. *Ecol Indic* 11:1552–1562. <https://doi.org/10.1016/j.ecolind.2011.03.025>